

**Potential variation around grain boundaries in BaSi<sub>2</sub> films grown on multicrystalline silicon evaluated using Kelvin probe force microscopy**

Masakazu Baba, Kosuke O. Hara, Daichi Tsukahara, Kaoru Toko, Noritaka Usami, Takashi Sekiguchi, and Takashi Suemasu

Citation: *Journal of Applied Physics* **116**, 235301 (2014); doi: 10.1063/1.4904864

View online: <http://dx.doi.org/10.1063/1.4904864>

View Table of Contents: <http://scitation.aip.org/content/aip/journal/jap/116/23?ver=pdfcov>

Published by the [AIP Publishing](#)

---

**Articles you may be interested in**

[Potential variations around grain boundaries in impurity-doped BaSi<sub>2</sub> epitaxial films evaluated by Kelvin probe force microscopy](#)

*J. Appl. Phys.* **116**, 123709 (2014); 10.1063/1.4896760

[Investigations on residual strains and the cathodoluminescence and electron beam induced current signal of grain boundaries in silicon](#)

*J. Appl. Phys.* **115**, 163511 (2014); 10.1063/1.4873958

[Evaluation of potential variations around grain boundaries in BaSi<sub>2</sub> epitaxial films by Kelvin probe force microscopy](#)

*Appl. Phys. Lett.* **103**, 142113 (2013); 10.1063/1.4824335

[Giant secondary grain growth in Cu films on sapphires](#)

*AIP Advances* **3**, 082105 (2013); 10.1063/1.4817829

[Large crystal grain niobium thin films deposited by energetic condensation in vacuum arc](#)

*J. Vac. Sci. Technol. A* **27**, 620 (2009); 10.1116/1.3131725

---



**AIP** | Journal of Applied Physics

**Meet The New Deputy Editors**

	<b>Christian Brosseau</b>		<b>Laurie McNeil</b>		<b>Simon Phillpot</b>
---	---------------------------	---	----------------------	---	-----------------------

## Potential variation around grain boundaries in BaSi<sub>2</sub> films grown on multicrystalline silicon evaluated using Kelvin probe force microscopy

Masakazu Baba,<sup>1</sup> Kosuke O. Hara,<sup>2</sup> Daichi Tsukahara,<sup>1</sup> Kaoru Toko,<sup>1</sup> Noritaka Usami,<sup>2,3</sup> Takashi Sekiguchi,<sup>4</sup> and Takashi Suemasu<sup>1,3</sup>

<sup>1</sup>*Institute of Applied Physics, University of Tsukuba, Tsukuba, Ibaraki 305-8573, Japan*

<sup>2</sup>*Graduate School of Engineering, Nagoya University, Nagoya 464-8603, Japan*

<sup>3</sup>*Japan Science and Technology Agency, CREST, Chiyoda, Tokyo 102-0075, Japan*

<sup>4</sup>*National Institute for Materials Science, Tsukuba, Ibaraki 305-0044, Japan*

(Received 1 October 2014; accepted 9 December 2014; published online 19 December 2014)

Potential variations across the grain boundaries (GBs) in a 100 nm thick undoped n-BaSi<sub>2</sub> film on a cast-grown multicrystalline Si (mc-Si) substrate are evaluated using Kelvin probe force microscopy (KFM). The  $\theta$ -2 $\theta$  X-ray diffraction pattern reveals diffraction peaks, such as (201), (301), (410), and (411) of BaSi<sub>2</sub>. Local-area electron backscatter diffraction reveals that the *a*-axis of BaSi<sub>2</sub> is tilted slightly from the surface normal, depending on the local crystal plane of the mc-Si. KFM measurements show that the potentials are not significantly disordered in the grown BaSi<sub>2</sub>, even around the GBs of mc-Si. The potentials are higher at GBs of BaSi<sub>2</sub> around Si GBs that are formed by grains with a Si(111) face and those with faces that deviate slightly from Si(111). Thus, downward band bending occurs at these BaSi<sub>2</sub> GBs. Minority carriers (holes) undergo a repelling force near the GBs, which may suppress recombination as in the case of undoped n-BaSi<sub>2</sub> epitaxial films on a single crystal Si(111) substrate. The barrier height for hole transport across the GBs varies in the range from 10 to 55 meV. The potentials are also higher at the BaSi<sub>2</sub> GBs grown around Si GBs composed of grains with Si(001) and Si(111) faces. The barrier height for hole transport ranges from 5 to 55 meV. These results indicate that BaSi<sub>2</sub> GBs formed on (111)-dominant Si surfaces do not have a negative influence on the minority-carrier properties, and thus BaSi<sub>2</sub> formed on underlayers, such as (111)-oriented Si or Ge and on (111)-oriented mc-Si, can be utilized as a solar cell active layer. © 2014 AIP Publishing LLC. [<http://dx.doi.org/10.1063/1.4904864>]

### I. INTRODUCTION

Both the band gap and absorption coefficient are key parameters for achieving high conversion efficiency in thin-film solar cells. We have focused on semiconducting barium disilicide (BaSi<sub>2</sub>) as an active layer to realize our target of *pn* junction solar cells. BaSi<sub>2</sub> consists of earth-abundant elements and has a suitable band gap of approximately 1.3 eV, and a high absorption coefficient that reaches  $3 \times 10^4 \text{ cm}^{-1}$  at 1.5 eV, despite its indirect band gap nature.<sup>1,2</sup> The high absorption coefficients originate from the localized Ba *d*-like states in the conduction band of BaSi<sub>2</sub>.<sup>3–5</sup> In addition, both the minority-carrier lifetime (*ca.* 10  $\mu\text{s}$ )<sup>6–8</sup> and the minority-carrier diffusion length (*ca.* 10  $\mu\text{m}$ )<sup>9,10</sup> in undoped n-type BaSi<sub>2</sub> epitaxial films on Si(111) are sufficiently large for thin-film solar cell applications. Kelvin probe force microscopy (KFM) measurements indicate the electrostatic potential variations across the grain boundaries (GBs) and are thus used to determine the band diagrams around the GBs. Such GBs in semiconductor films often degrade the electrical and optical properties of the films. Therefore, extensive studies have been conducted on GBs in solar cell materials, such as polycrystalline Si and chalcopyrite semiconductors in an attempt to improve efficiency.<sup>11–31</sup> According to our previous investigations,<sup>32,33</sup> the electrostatic potentials were higher at GBs in undoped n-BaSi<sub>2</sub> and lightly Sb-doped n-BaSi<sub>2</sub> epitaxial films on Si(111) than those in the BaSi<sub>2</sub> grain interiors by approximately 10–30 mV. This downward

band bending at the GBs is beneficial for n-type BaSi<sub>2</sub>, because the minority carriers (holes) are not attracted toward the GBs, which enable the suppression of minority-carrier recombination at the GBs. This accounts for the much larger minority-carrier diffusion length (*ca.* 10  $\mu\text{m}$ ) than that for the average grain size of undoped n-BaSi<sub>2</sub> epitaxial films (*ca.* 0.2  $\mu\text{m}$ ).<sup>9</sup> In contrast, upward band bending occurs at the GBs in undoped n-BaSi<sub>2</sub> epitaxial films on Si(001),<sup>32</sup> which results in a smaller minority-carrier diffusion length (*ca.* 1.5  $\mu\text{m}$ ).<sup>10</sup> Therefore, the potential variations around the GBs is a measure of the minority-carrier properties in BaSi<sub>2</sub> films.

However, all of these properties have been measured for *a*-axis-oriented BaSi<sub>2</sub> epitaxial films grown on single-crystal Si(111) or Si(001) substrates. It is of significant interest to determine the potential variations in BaSi<sub>2</sub> formed on multicrystalline Si (mc-Si) substrates, especially those around the GBs of the mc-Si substrate. This would provide information on the potential application of a BaSi<sub>2</sub> single-junction solar cell on an inexpensive SiO<sub>2</sub> substrate covered with (111)-oriented polycrystalline Si or Ge layers by Al-induced crystallization (AIC),<sup>34–38</sup> and multijunction or heterojunction solar cells composed of wider band gap (Ba,Sr)(Si,C)<sub>2</sub> silicides<sup>39–43</sup> and mc-Si. This article reports the growth of BaSi<sub>2</sub> layers on a mc-Si substrate by molecular beam epitaxy (MBE), and discusses the crystal orientation determined by X-ray diffraction (XRD) and electron backscatter diffraction (EBSD) analyses, and the surface potential distribution around BaSi<sub>2</sub> GBs determined from KFM.

## II. EXPERIMENTAL PROCEDURE

An ion-pumped MBE system equipped with a standard Knudsen cell for Ba and an electron-beam evaporation source for Si was employed. A cast-grown mc-Si substrate<sup>44</sup> was used to grow a 100 nm thick undoped n-BaSi<sub>2</sub> film. The growth procedures are briefly described as follows.<sup>45,46</sup> A two-step growth method was employed using reactive deposition epitaxy (RDE) and subsequent MBE. After cleaning the mc-Si in an ultrahigh vacuum, the substrate temperature  $T_S$ , Ba deposition rate  $R_{Ba}$ , and the growth time  $t$ , were set at 580 °C, 1 nm/min, and 5 min, respectively, to form an approximately 10 nm thick BaSi<sub>2</sub> template layer. The BaSi<sub>2</sub> template acts as seed crystals for subsequent overlayers. Next, the conditions were set to  $T_S = 650$  °C,  $R_{Ba} = 3$  nm/min, a Si deposition rate of  $R_{Si} = 1$  nm/min, and  $t = 60$  min, for the formation of a 100 nm thick BaSi<sub>2</sub> film. The conditions employed were suitable for the growth of BaSi<sub>2</sub> epitaxial films on a Si(111) surface. Although *a*-axis oriented BaSi<sub>2</sub> epitaxial films can be grown on both Si(111) and Si(001),<sup>47,48</sup> the optimum growth temperatures for these processes are different.

The crystalline quality of the grown film was characterized using  $\theta$ - $2\theta$  XRD with a Cu K $\alpha$  radiation source. The crystal orientation of BaSi<sub>2</sub> and mc-Si was analyzed using EBSD with an acceleration voltage of 20 kV. The measurement areas for EBSD were  $2 \times 2$  mm<sup>2</sup> and  $12.5 \times 12.5$   $\mu$ m<sup>2</sup> with step sizes of 20 and 0.1  $\mu$ m, respectively. Inverse pole figure maps and pole figures were produced from the crystal orientation data. For the pole figures, the orientation distribution function was calculated by spherical harmonic series expansion ( $L = 16$ ), followed by Gaussian smoothing with a half width of 5°. Surface topographies and electrostatic potential variations were investigated using Shimadzu SPM-9600 atomic force microscopy (AFM) and KFM, respectively.

## III. RESULT AND DISCUSSION

Figure 1 shows the  $\theta$ - $2\theta$  XRD pattern for the sample, with diffraction peaks, such as (201), (301), (410), and (411) of BaSi<sub>2</sub>. These planes are tilted slightly from the (100)

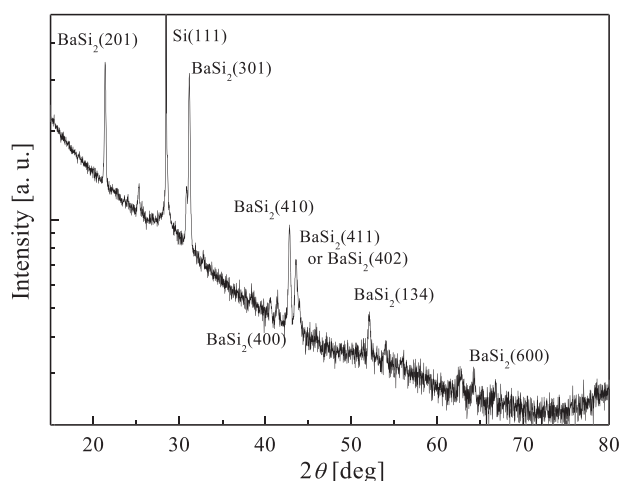


FIG. 1.  $\theta$ - $2\theta$  XRD pattern of the sample. The layer thickness of BaSi<sub>2</sub> is approximately 100 nm.

plane of BaSi<sub>2</sub>. Figure 2(a) shows an optical microscope image of the sample, where GBs are clearly evident, even after the growth of BaSi<sub>2</sub>. Figures 2(b) and 2(c) present EBSD inverse pole figure maps together with a grey-scale image of BaSi<sub>2</sub> and the mc-Si substrate, respectively. The inverse pole figure map in Fig. 2(c) was acquired after etching the BaSi<sub>2</sub> layer with hydrofluoric acid. Approximately, half the BaSi<sub>2</sub> surface appears green in Fig. 2(b), whereas the upper left and lower left areas are dark, which indicates the difficulty in determining the crystal orientation. Kikuchi patterns for BaSi<sub>2</sub> were not clearly observed in these dark areas due to surface roughness. The green areas in Fig. 2(b) correspond to *a*-axis oriented BaSi<sub>2</sub> grains, where the *a*-axis oriented BaSi<sub>2</sub> in areas I and V was formed on the Si grains (blue areas in Fig. 2(c)), which are (111)-plane surfaces. However, the green colors in areas III and IV are slightly different from those in areas I and V, as is evident in Fig. 2(b). In these areas, the crystal orientation of the Si grains is tilted slightly from the (111) plane toward the (001) plane, as shown in Fig. 2(c), which results in deterioration of the *a*-axis orientation of the BaSi<sub>2</sub> film. A pole-figure analysis was performed to examine the perpendicularity of the BaSi<sub>2</sub> *a*-axis from a microscopic perspective, and the results are shown in Fig. 3. The left and right rows show the pole figures for BaSi<sub>2</sub>(100)

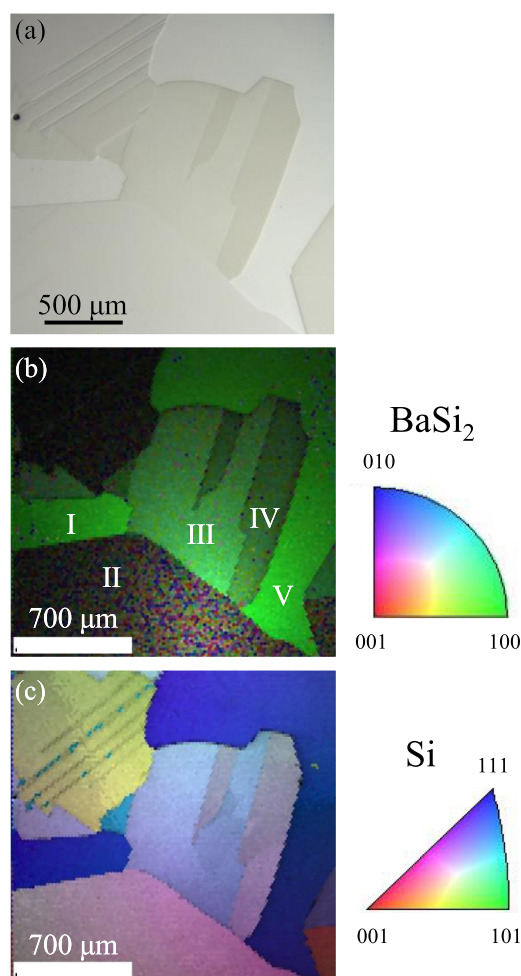


FIG. 2. (a) Optical microscope image and EBSD inverse pole figure maps superimposed with grey-scale image quality of the (b) BaSi<sub>2</sub> film and (c) mc-Si. The color keys indicate crystal orientation.

and  $\text{BaSi}_2(001)$ , respectively, generated from the EBSD map in Fig. 2(b). Figures 3(a)–3(e) correspond to the  $12.5 \times 12.5 \mu\text{m}^2$  selected areas in areas I–V of Fig. 2(b), respectively. In Figs. 3(a)–3(e), the red area is almost in the center of the left row for the pole figures of areas I, II, and V, which indicates that the  $a$ -axis of  $\text{BaSi}_2$  is normal to the sample surface. However, the peak intensity for  $\text{BaSi}_2$  in area II, which was grown on a Si grain with the crystal face inclined slightly from (001), is much smaller than those in areas I and V. This is because the conditions employed were not suitable for  $\text{BaSi}_2$  growth on Si(001). The red areas appear on the circumference of the right row pole figures for areas I and V, and these correspond to the presence of three epitaxial variants of  $\text{BaSi}_2$ . This result is consistent with those obtained for  $\text{BaSi}_2$  epitaxial films on single crystal Si(111) substrates.<sup>46,49</sup> In Figs. 3(c) and 3(d), the red areas are displaced from the center, which indicates that the  $a$ -axis of  $\text{BaSi}_2$  is

tilted from the surface normal by a small angle ( $\approx 10^\circ$ ) in areas III and IV. The XRD peaks, such as (201), (301), and (401) of  $\text{BaSi}_2$  in Fig. 1, are attributed to these tilted  $\text{BaSi}_2$  planes.

Next, the potential variations around the GBs in  $\text{BaSi}_2$  were investigated. Figures 4(a) and 4(b) present AFM topographic and KFM surface potential images, respectively, for the  $\text{BaSi}_2$  film on (111)-face dominant Si grains, where the observation area was  $5 \times 5 \mu\text{m}^2$ . The white dashed (GB-1) and dotted (GB-2) lines indicate the positions of the mc-Si GBs. In Fig. 4(a), areas i and ii denote the upper and left areas surrounded by GB-1 and GB-2, and area iii is the lower right part separated by GB-2. Figures 4(c) and 4(d) show cross-sectional profiles of the AFM and KFM images along lines AA' and BB', in Figs. 4(a) and 4(b). These line scans were performed across GB-1 and GB-2. The surface

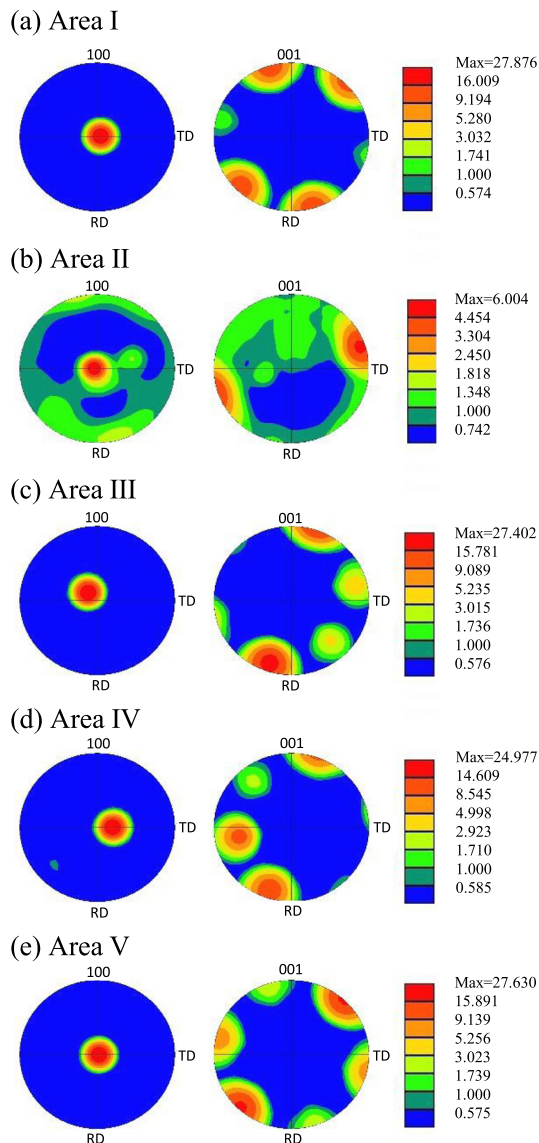


FIG. 3. (100) and (001) pole figures of  $\text{BaSi}_2$  for areas (a) I, (b) II, (c) III, (d) IV, and (e) V shown in Fig. 2(b), produced from the crystal orientation data obtained from EBSD measurements. The symbols TD and RD denote the transverse and reference directions, respectively. Relative intensities are also shown.

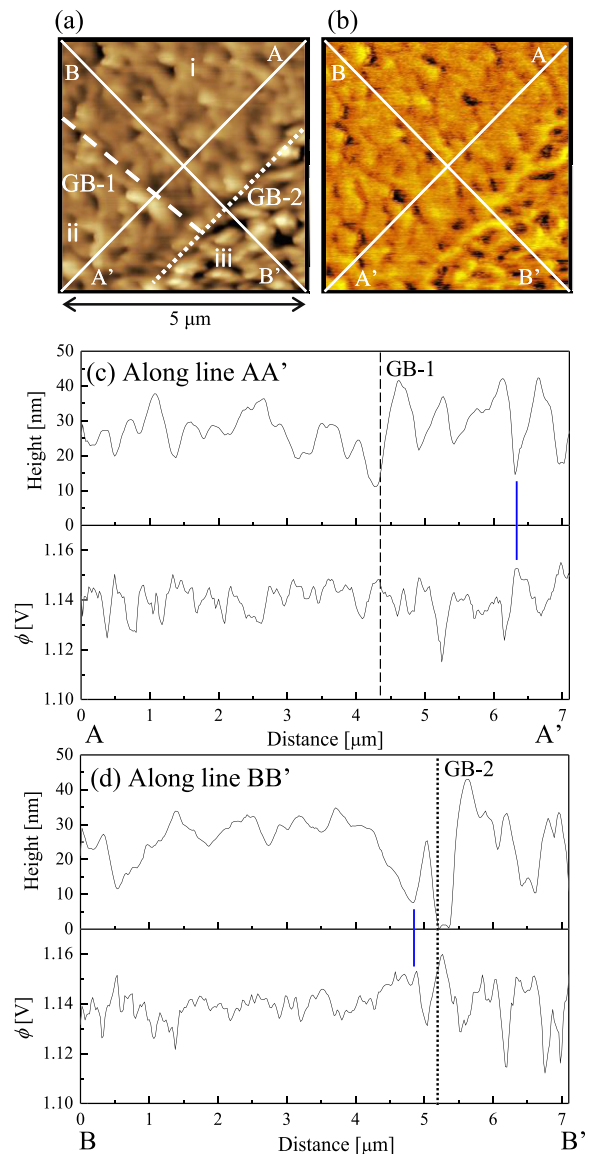


FIG. 4. (a) AFM topographic and (b) KFM surface potential images for the  $\text{BaSi}_2$  film on mc-Si with a (111) face, observed in the same  $5 \times 5 \mu\text{m}^2$  area. The white dashed (GB-1) and dotted (GB-2) lines indicate the positions of GBs in the mc-Si. AFM and KFM cross-sections along (c) line AA' and (d) line BB' shown in (a). The blue lines are given as guides to indicate the appearance of inversion.

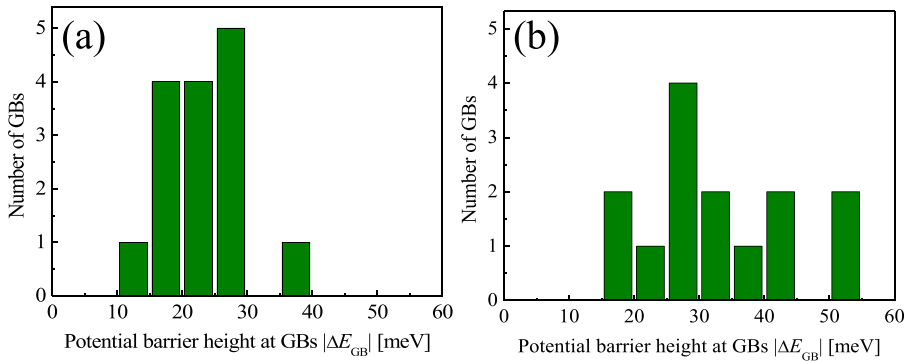


FIG. 5. Histograms of barrier height for hole transport in BaSi<sub>2</sub> across (a) GB-1 and (b) GB-2.

morphologies of BaSi<sub>2</sub> in area iii appear to be different from those in area i, as shown in Fig. 4(d). The surface in area iii is rough, whereas the other areas are relatively smooth. This difference is due to the small tilt of the mc-Si surface from the actual (111) plane in area iii. The cross-sectional profiles of the AFM and KFM images in Figs. 4(c) and 4(d) appear to be inversions of each other. This means that the surface potentials increase at the GBs with respect to those in the grain interiors of BaSi<sub>2</sub>, which indicates that the GBs are positively charged, and thereby a downward band bending occurs at the GBs. Note that the potentials are also higher at the GBs of BaSi<sub>2</sub> formed around the GBs of the mc-Si, as denoted by the dashed line (GB-1) in Fig. 4(c) and the dotted line (GB-2) in Fig. 4(d). The same trend was observed in other areas of the BaSi<sub>2</sub> formed on the (111)-face dominant Si grains. This band bending is beneficial for n-type BaSi<sub>2</sub> because the minority carriers (holes) are not attracted toward the GBs, and therefore the recombination of minority carriers may be suppressed. This is also found for undoped n-BaSi<sub>2</sub> epitaxial films on a single crystalline Si(111) substrate.<sup>32</sup> Figures 5(a) and 5(b) show histograms of the barrier height for hole transport in BaSi<sub>2</sub> across GB-1 and GB-2, respectively. The potential barrier height  $\Delta E_{GB}$ , at GBs was evaluated using

$$\Delta E_{GB} = -q(V_{GB} - V_{G,ave}), \quad (1)$$

where  $V_{GB}$  and  $V_{G,ave}$  are the potential at GBs and the average potential in the inner parts of two adjoining grains, respectively, and  $q$  denotes the elementary charge. The same procedure was repeated for approximately 15 GBs. The barrier height for hole transport at the GBs was in the range from *ca.* 10 to 40 meV for GB-1, and from *ca.* 15 to 55 meV for GB-2. Although these barrier heights are slightly larger than those for BaSi<sub>2</sub> on single-crystal Si(111) (10–30 meV), such barrier heights are still of the same order as the thermal energy at room temperature and thereby may not deteriorate the carrier transport properties.

Figures 6(a) and 6(b) show AFM topographic and KFM surface potential images, respectively, for the BaSi<sub>2</sub> film on a (001)-face Si grain in the upper left, and on a (111)-face Si grain in the lower right. The observation area was  $15 \times 15 \mu\text{m}^2$ . The white dashed line in Fig. 6(a) shows the position of the mc-Si GB (GB-3) with elongated BaSi<sub>2</sub> grains evident in the upper left, which are specific to BaSi<sub>2</sub> formed on vicinal Si(001).<sup>50</sup> Figure 6(c) shows cross-sectional

profiles of the AFM and KFM images along the line CC' shown in Fig. 6(a). The line scan was performed across GB-3. The cross-sectional profiles of AFM and KFM images appear to be inversions of each other for BaSi<sub>2</sub> grown on the (111)-face Si, as shown in the right part of Fig. 6(c). Note that the potential is also higher in BaSi<sub>2</sub> at GB-3, as denoted by the dashed line in Fig. 6(c). The same tendency was observed in other areas of the sample. The barrier height for hole transport in BaSi<sub>2</sub> across GB-3 was in the range from *ca.* 5 to 55 meV, as shown in Fig. 7. Such barrier heights are not likely to deteriorate carrier transport across the GBs. On

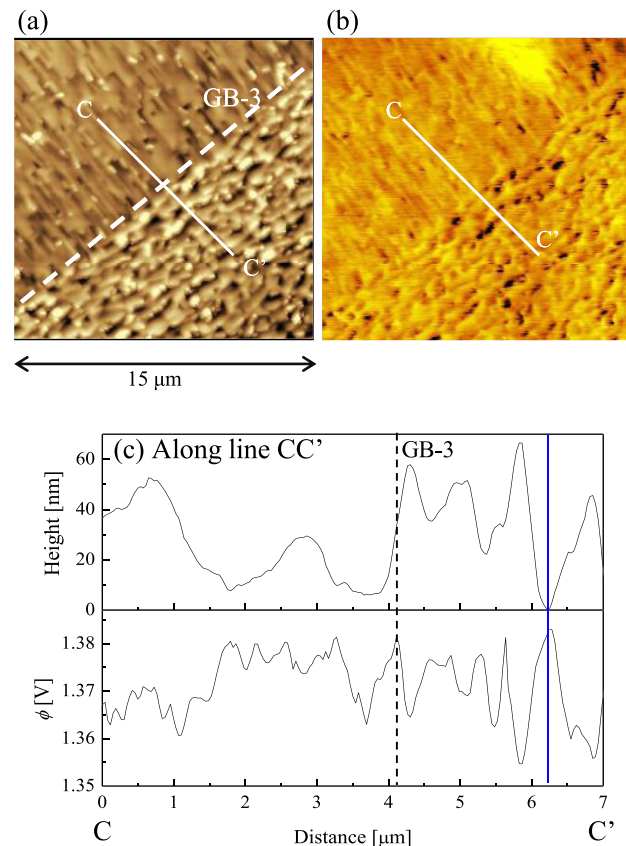


FIG. 6. (a) AFM topographic and (b) KFM surface potential images for the BaSi<sub>2</sub> film on the mc-Si observed in the same  $5 \times 5 \mu\text{m}^2$  area. The white dashed line (GB-3) shows the position of the GB in the mc-Si. The crystal planes of the upper left and lower right of the mc-Si are Si(001) and Si(111) faces, respectively. (c) AFM and KFM cross-sections along the white line CC'. The blue line is a guide to indicate the appearance of inversion.

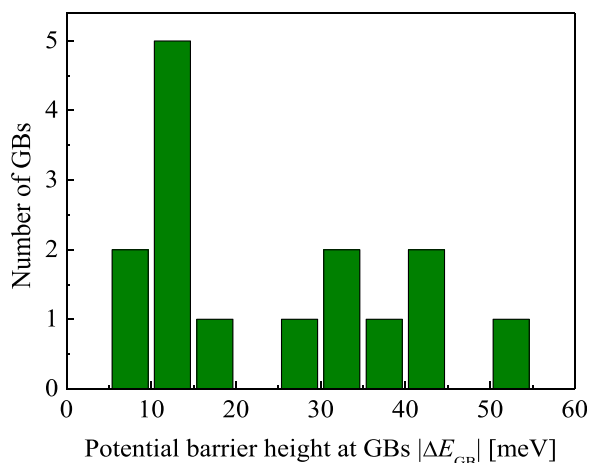


FIG. 7. Histogram of barrier height for hole transport in BaSi<sub>2</sub> across GB-3.

the basis of these results, it was concluded that the BaSi<sub>2</sub> GBs formed around Si grains with (111)-dominant surfaces do not have a negative influence on the minority-carrier properties in the BaSi<sub>2</sub> film, with respect to their potential variations. These results suggest the potential of BaSi<sub>2</sub> layers on (111)-oriented polycrystalline Si underlayers formed on SiO<sub>2</sub> and those on (111)-oriented mc-Si for solar cell applications.

#### IV. CONCLUSION

A 100 nm thick undoped n-BaSi<sub>2</sub> film was formed by MBE on a cast-grown mc-Si substrate, and the potential variations around the GBs were evaluated using KFM. Measurements of local-area EBSD revealed that the *a*-axis of BaSi<sub>2</sub> was tilted from the surface normal, depending on the local crystal plane of the mc-Si. The potentials were higher at the GBs of BaSi<sub>2</sub> formed on the grain interiors or on the GBs of mc-Si, where the (111) face was dominant. The barrier height for hole transport across the GBs ranged from *ca.* 10 to 55 meV. This band structure repulses minority carriers (holes) at the GBs of BaSi<sub>2</sub>, and therefore is preferable for the suppression of carrier recombination. The same was true for BaSi<sub>2</sub> around Si GBs that consist of grains with Si(001) and Si(111) faces, where the barrier height for hole transport ranged from *ca.* 5 to 55 meV. These results clearly demonstrate that BaSi<sub>2</sub> films formed on (111)-dominant Si surfaces of mc-Si or those produced by AIC have potential for solar cell applications.

#### ACKNOWLEDGMENTS

This work was financially supported in part by the Core Research for Evolutionary Science and Technology (CREST) program of the Japan Science and Technology Agency (JST).

- <sup>1</sup>K. Morita, Y. Inomata, and T. Suemasu, *Thin Solid Films* **508**, 363 (2006).  
<sup>2</sup>K. Toh, T. Saito, and T. Suemasu, *Jpn. J. Appl. Phys. Part 1* **50**, 068001 (2011).  
<sup>3</sup>Y. Imai, A. Watanabe, and M. Mukaida, *J. Alloys Compd.* **358**, 257 (2003).

- <sup>4</sup>D. B. Migas, V. L. Shaposhnikov, and V. E. Borisenko, *Phys. Status Solidi B* **244**, 2611 (2007).  
<sup>5</sup>M. Kumar, N. Umezawa, and M. Imai, *Appl. Phys. Express* **7**, 071203 (2014).  
<sup>6</sup>K. O. Hara, N. Usami, K. Toh, M. Baba, T. Toko, and T. Suemasu, *J. Appl. Phys.* **112**, 083108 (2012).  
<sup>7</sup>K. O. Hara, N. Usami, K. Nakamura, R. Takabe, M. Baba, K. Toko, and T. Suemasu, *Appl. Phys. Express* **6**, 112302 (2013).  
<sup>8</sup>R. Takabe, K. O. Hara, M. Baba, W. Du, N. Shimada, K. Toko, N. Usami, and T. Suemasu, *J. Appl. Phys.* **115**, 193510 (2014).  
<sup>9</sup>M. Baba, K. Toh, K. Toko, N. Saito, N. Yoshizawa, K. Jiptner, T. Sakiguchi, K. O. Hara, N. Usami, and T. Suemasu, *J. Cryst. Growth* **348**, 75 (2012).  
<sup>10</sup>M. Baba, K. Watanabe, K. O. Hara, K. Toko, T. Sekiguchi, N. Usami, and T. Suemasu, *Jpn. J. Appl. Phys. Part 1* **53**, 078004 (2014).  
<sup>11</sup>C. H. Seager and G. E. Pike, *Appl. Phys. Lett.* **35**, 709 (1979).  
<sup>12</sup>M. Spencer, R. Stall, L. F. Eastman, and C. E. C. Wood, *J. Appl. Phys.* **50**, 8006 (1979).  
<sup>13</sup>J. J. Yang, P. D. Dapkus, R. D. Dupuis, and R. Do. Yingling, *J. Appl. Phys.* **51**, 3794 (1980).  
<sup>14</sup>J. Werner, W. Jantsch, and H. J. Queisser, *Solid State Commun.* **42**, 415 (1982).  
<sup>15</sup>D. P. Joshi and D. P. Bhatt, *Sol. Energy Mater. Sol. Cells* **22**, 137 (1991).  
<sup>16</sup>R. Rizk and G. Nouet, *Interface Sci.* **4**, 303 (1996).  
<sup>17</sup>I. Visoly-Fisher, S. R. Cohen, and D. Cahen, *Appl. Phys. Lett.* **82**, 556 (2003).  
<sup>18</sup>J. Chen, T. Sekiguchi, D. Yang, F. Yin, K. Kido, and S. Tsurekawa, *J. Appl. Phys.* **96**, 5490 (2004).  
<sup>19</sup>C.-S. Jiang, R. Noufi, K. Ramanathan, J. A. AbuShama, H. R. Moutinho, and M. M. Al-Jassim, *Appl. Phys. Lett.* **85**, 2625 (2004).  
<sup>20</sup>D. F. Marrón, S. Sadewasser, A. Meeder, Th. Glatzel, and M. Ch. Lux-Steiner, *Phys. Rev. B* **71**, 033306 (2005).  
<sup>21</sup>S. Tsurekawa, K. Kido, and T. Watanabe, *Philos. Mag. Lett.* **85**, 41 (2005).  
<sup>22</sup>M. J. Hetzer, Y. M. Strzhemechny, M. Gao, M. A. Contreras, A. Zunger, and L. J. Brillson, *Appl. Phys. Lett.* **86**, 162105 (2005).  
<sup>23</sup>M. Gloeckler, J. R. Sites, and W. K. Metzger, *J. Appl. Phys.* **98**, 113704 (2005).  
<sup>24</sup>G. Hanna, T. Glatzel, S. Sadewasser, N. Ott, H. P. Strunk, U. Rau, and J. H. Werner, *Appl. Phys. A* **82**, 1 (2006).  
<sup>25</sup>S. Tsurekawa, K. Kido, and T. Watanabe, *Mater. Sci. Eng. A* **462**, 61 (2007).  
<sup>26</sup>M. Kawamura, T. Yamada, N. Suyama, A. Yamada, and M. Konagai, *Jpn. J. Appl. Phys. Part 1* **49**, 062301 (2010).  
<sup>27</sup>S. Oonishi, M. Kawamura, N. Takano, D. Hashimoto, A. Yamada, and M. Konagai, *Thin Solid Films* **519**, 7347 (2011).  
<sup>28</sup>T. Minemoto, Y. Wakisaka, and H. Takakura, *Jpn. J. Appl. Phys. Part 1* **50**, 031203 (2011).  
<sup>29</sup>D. R. Kim, C. H. Lee, J. M. Weisse, I. S. Cho, and X. Zheng, *Nano Lett.* **12**, 6485 (2012).  
<sup>30</sup>Z. Zhang, X. Tang, O. Kiowski, M. Hetterich, U. Lemmer, M. Powalla, and H. Hölscher, *Appl. Phys. Lett.* **100**, 203903 (2012).  
<sup>31</sup>M. Takihara, T. Minemoto, Y. Wakisaka, and T. Takahashi, *Prog. Photovoltaics* **21**, 595 (2013).  
<sup>32</sup>M. Baba, S. Tsurekawa, K. Watanabe, W. Du, K. Toko, K. O. Hara, N. Usami, T. Sekiguchi, and T. Suemasu, *Appl. Phys. Lett.* **103**, 142113 (2013).  
<sup>33</sup>D. Tsukahara, M. Baba, S. Honda, Y. Imai, K. O. Hara, N. Usami, K. Toko, J. H. Werner, and T. Suemasu, *J. Appl. Phys.* **116**, 123709 (2014).  
<sup>34</sup>O. Nast, T. Puzzer, L. M. Koschier, A. B. Sproul, and S. R. Wenham, *Appl. Phys. Lett.* **73**, 3214 (1998).  
<sup>35</sup>D. Tsukada, Y. Matsumoto, R. Sasaki, M. Takeishi, T. Saito, N. Usami, and T. Suemasu, *Appl. Phys. Express* **2**, 051601 (2009).  
<sup>36</sup>K. Toko, M. Kurosawa, N. Saitoh, N. Yoshizawa, N. Usami, M. Miyao, and T. Suemasu, *Appl. Phys. Lett.* **101**, 072106 (2012).  
<sup>37</sup>R. Numata, K. Toko, N. Saitoh, N. Yoshizawa, N. Usami, and T. Suemasu, *Cryst. Growth Des.* **13**, 1767 (2013).  
<sup>38</sup>K. Toko, R. Numata, N. Saitoh, N. Yoshizawa, N. Usami, and T. Suemasu, *J. Appl. Phys.* **115**, 094301 (2014).  
<sup>39</sup>Y. Inomata, T. Suemasu, T. Izawa, and F. Hasegawa, *Jpn. J. Appl. Phys. Part 2* **43**, L771 (2004).  
<sup>40</sup>K. Morita, M. Kobayashi, and T. Suemasu, *Jpn. J. Appl. Phys. Part 2* **45**, L390 (2006).  
<sup>41</sup>Y. Imai and A. Watanabe, *Thin Solid Films* **515**, 8219 (2007).

- <sup>42</sup>Y. Imai and A. Watanabe, *Intermetallics* **18**, 1432 (2010).
- <sup>43</sup>M. Kumar, N. Umezawa, and M. Imai, *J. Appl. Phys.* **115**, 203718 (2014).
- <sup>44</sup>R. R. Prakash, T. Sekiguchi, K. Jiptner, Y. Miyamura, J. Chen, H. Harada, and K. Kakimoto, *J. Cryst. Growth* **401**, 717 (2014).
- <sup>45</sup>Y. Inomata, T. Nakamura, T. Suemasu, and F. Hasegawa, *Jpn. J. Appl. Phys. Part 1* **43**, 4155 (2004).
- <sup>46</sup>Y. Inomata, T. Nakamura, T. Suemasu, and F. Hasegawa, *Jpn. J. Appl. Phys. Part 2* **43**, L478 (2004).
- <sup>47</sup>R. A. McKee, F. J. Walker, J. R. Conner, and R. Raj, *Appl. Phys. Lett.* **63**, 2818 (1993).
- <sup>48</sup>K. Toh, K. O. Hara, N. Usami, N. Saito, N. Yoshizawa, K. Toko, and T. Suemasu, *J. Cryst. Growth* **345**, 16 (2012).
- <sup>49</sup>R. Takabe, K. Nakamura, M. Baba, W. Du, M. Ajmal Khan, K. Toko, M. Sasase, K. O. Hara, N. Usami, and T. Suemasu, *Jpn. J. Appl. Phys. Part 1* **53**, 04ER04 (2014).
- <sup>50</sup>K. Toh, K. O. Hara, N. Usami, N. Saito, N. Yoshizawa, K. Toko, and T. Suemasu, *Jpn. J. Appl. Phys. Part 1* **51**, 095501 (2012).